

Adaptive Test-Time Defense with the Manifold Hypothesis

Zhaoyuan Yang¹, Zhiwei Xu², Jing Zhang², Richard Hartley², Peter Tu¹

¹GE Research, ²The Australian National University

{zhaoyuan.yang,tu}@ge.com, {zhiwei.xu,jing.zhang,richard.hartley}@anu.edu.au

Abstract

In this work, we formulate a novel framework of adversarial robustness using the manifold hypothesis. Our framework provides sufficient conditions for defending against adversarial examples. We develop a test-time defense method with variational inference and our formulation. The developed approach combines manifold learning with variational inference to provide adversarial robustness without the need for adversarial training. We show that our approach can provide adversarial robustness even if attackers are aware of the existence of test-time defense. In addition, our approach can also serve as a test-time defense mechanism for variational autoencoders.

1. Introduction

State-of-the-art neural network models are known to suffer from adversarial examples. With small perturbations, adversarial examples can completely change predictions of neural networks [32]. Common defense methods for adversarial attacks include adversarial training [19], certified robustness [35], etc.

Recently, test-time defenses of adversarial examples, which optimize at test time, have drawn increasing attention [4]. In this work, we present a novel theoretical framework of test-time defenses with the assumption that high-dimensional images lie on low-dimensional manifolds (the manifold hypothesis). Compared with low-dimensional data, high-dimensional data are more vulnerable to adversarial examples [7]. Therefore, we transform adversarial robustness from a high-dimensional problem to a low-dimensional problem, and present a novel test-time defense method for non-adversarially trained models via manifold learning and variational inference. With our method, non-adversarially trained models can achieve performance on par with the performance of adversarially trained models. Even if attackers are aware of the existence of test-time defenses, our approach can still provide adversarial robustness against attacks. The **main contributions** of our work are: **1)** A novel framework for adversarial defense with the manifold hypothesis;

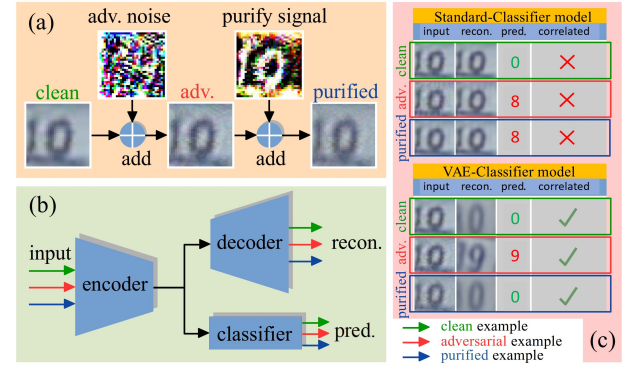


Figure 1. Test-time defense against adversarial attacks. (a) visualization of clean, adversarial and purified images. The adversarial noise and the purified signal are multiplied by 30 for better visualization. (b) joint learning of variational autoencoder and classification. (c) semantic correlation between prediction and reconstruction. Predictions and reconstructions are normal on clean images but abnormal on adversarial images. For the VAE-classifier model, the classifier is strongly correlated with the decoder due to the semantic correlation in the prediction and the reconstruction.

2) A novel and effective test-time defense approach which combines manifold learning and variational inference.

2. Related Work

There have been extensive efforts in defending against adversarial attacks on neural networks. We describe works related to our approach from adversarial training to adversarial purification, and then the use of variational inference to defend against adversarial attacks.

Adversarial Training: Adversarial training is one of the most effective attack defense methods. This method introduces adversarial examples in the train set during training [7, 19]. It has been shown that adversarial training can degrade classification accuracy of models on clean data [33]. To reduce the degradation in clean classification accuracy, Trades [38] is proposed to balance the trade-off between clean and robust accuracy. Recent efforts also study the

impact of different hyperparameters [22] as well as data augmentation [25] to reduce the effect of robust overfitting, where robust test accuracy decreases during training. Besides the standard adversarial training, some works study the impacts of adversarial training on manifolds as well [18, 23, 31, 39]. In this work, we present a novel test-time defense method without adversarial training.

Adversarial Purification: As an alternative to adversarial training, adversarial purification aims to shift adversarial examples back to representations of clean examples during test time. There have been efforts that study adversarial purification methods using GAN-based models [27], energy-based models [8, 10, 37], *etc.* The test-time defense method presented in this work is close to formulations of PixelDefend [30], SOAP [29] and Mao et al. [20]. PixelDefend discovers that adversarial examples lie in low probability regions. It uses a PixelCNN model to restore adversarial examples back to high probability regions. SOAP [29] and Mao et al. [20] discover that adversarial attacks will increase the loss of self-supervised learning objectives and they define reverse vectors based on that to reverse adversarial examples. In this work, we present a novel test-time defense objective combining manifold learning and variational inference to defend against adversarial examples.

Variational Inference based Attack Defense: Variational AutoEncoders (VAEs) [13] approximate the true posterior with an approximate posterior for probability density estimation in latent space. It has been shown that VAEs are vulnerable to adversarial attacks [14]. Many efforts have attempted to address this problem by, for instance, purifying adversarial examples with class manifold projection [11, 28], rejecting adversarial examples with Gaussian mixture components [6], disentangling latent representations of hierarchical VAEs [34], adversarial training of VAEs [17], *etc.* The presented method in this work can also be considered as a test-time defense method of VAE models.

3. Defending Adversarial Examples with the Manifold Hypothesis

We now present a novel framework of adversarial robustness and develop a test-time defense method to validate our framework. Let \mathcal{D}_{XY} be the set of clean images and their labels. The set consists of image-label pairs $(\mathbf{x}, \mathbf{y}) \in \mathcal{D}_{XY}$. Our framework is based on the manifold hypothesis which states that many real-world high-dimensional data $\mathbf{x} \in \mathbb{R}^n$ lies on a low-dimensional manifold \mathcal{M} diffeomorphic to \mathbb{R}^m with $m < n$. We define an encoder function $\mathbf{f} : \mathbb{R}^n \rightarrow \mathbb{R}^m$ and a decoder function $\mathbf{f}^\dagger : \mathbb{R}^m \rightarrow \mathbb{R}^n$ that together make an autoencoder. Thus, \mathbf{f} is a function that maps a data point $\mathbf{x} \in \mathbb{R}^n$ to a point $\mathbf{f}(\mathbf{x}) \in \mathbb{R}^m$. For a point $\mathbf{x} \in \mathcal{M}$, \mathbf{f}^\dagger and \mathbf{f} are approximate inverses. We lay out our theoretical formulation of a test-time defense framework below.

3.1. Problem Formulation

Given an image-label pairs $(\mathbf{x}, \mathbf{y}) \in \mathcal{D}_{XY}$ and a class label set $\mathcal{Y} = \{1, \dots, c\}$ where c is the number of classes, the encoder maps the image \mathbf{x} to a lower-dimensional vector $\mathbf{z} = \mathbf{f}(\mathbf{x})$. We then define a classifier in the latent space as $\mathbf{h} : \mathbb{R}^m \rightarrow \mathcal{Y}$. The encoder \mathbf{f} and \mathbf{h} together make the classifier in the input image space $\mathbf{y}_{\text{pred}} = \mathbf{h}(\mathbf{z}) = (\mathbf{h} \circ \mathbf{f})(\mathbf{x})$. In standard situations, the classifier predicts labels consistent with the ground truth labels such that $\mathbf{y}_{\text{pred}} = \mathbf{y}$. However, in adversarial situations, the adversary can generate a small adversarial perturbation δ_{adv} such that $\mathbf{y}_{\text{pred}} = (\mathbf{h} \circ \mathbf{f})(\mathbf{x}) \neq \mathbf{y}_{\text{adv}} = (\mathbf{h} \circ \mathbf{f})(\mathbf{x} + \delta_{\text{adv}})$. Adversarial perturbations $\delta_{\text{adv}} \in \mathbb{R}^n$ are required to be ℓ_p -bounded where $p = \{0, 2, \infty\}$ are common values. We aim to find a purified signal $\epsilon_{\text{pfy}} \in \mathbb{R}^n$ such that $(\mathbf{h} \circ \mathbf{f})(\mathbf{x}) = (\mathbf{h} \circ \mathbf{f})(\mathbf{x} + \delta_{\text{adv}} + \epsilon_{\text{pfy}}) = \mathbf{y}$. We let \mathbf{x} be the clean example, $\mathbf{x}_{\text{adv}} = \mathbf{x} + \delta_{\text{adv}}$ be the adversarial example and $\mathbf{x}_{\text{pfy}} = \mathbf{x}_{\text{adv}} + \epsilon_{\text{pfy}}$ be the purified example. If $\epsilon_{\text{pfy}} = -\delta_{\text{adv}}$, purification will be ideal and $\mathbf{x} = \mathbf{x}_{\text{pfy}}$; however, adversarial perturbation is unknown in real world. Therefore, we need to find an alternative approach to estimate the purified signal.

3.2. Theoretical Framework for Test-Time Defense with Manifold Learning

We define a robust classifier for image-label pairs $(\mathbf{x}, \mathbf{y}) \in \mathcal{D}_{XY}$ as $\mathbf{G}_R : \mathbb{R}^n \rightarrow \mathcal{Y}$, which yields a class prediction $\mathbf{y}_{\text{pred}} = \mathbf{G}_R(\mathbf{x})$ given an input image $\mathbf{x} \in \mathbb{R}^n$.

Definition 1. (*Robust classifier in the image space*) A robust classifier \mathbf{G}_R in the image space satisfies the following condition: for every image-label pair $(\mathbf{x}, \mathbf{y}) \in \mathcal{D}_{XY}$ and any perturbation vector $\boldsymbol{\eta} \in \mathbb{R}^n$ with $\|\boldsymbol{\eta}\|_p \leq \tau$, $\mathbf{y} = \mathbf{G}_R(\mathbf{x}) = \mathbf{G}_R(\mathbf{x} + \boldsymbol{\eta})$.

Perturbation budget τ is a threshold value for static semantic interpretations between \mathbf{x} and $(\mathbf{x} + \boldsymbol{\eta})$. For example, given a clean image \mathbf{x} with pixel values in $[0, 1]$, if $\|\boldsymbol{\eta}\|_\infty \leq 8/255$, then $(\mathbf{x} + \boldsymbol{\eta})$ belongs to the same class of \mathbf{x} . In other words, a perturbation with a ℓ_∞ -norm no greater than $8/255$ keep the image semantic interpretation unchanged in this example. τ varies on the type of ℓ_p -norm and can be much larger than $8/255$ in many real-world examples.

It is challenge to construct an adversarially robust model \mathbf{G}_R in the image space due to high-dimensional input space. In this work, we aim to find an alternative solution to match performance of \mathbf{G}_R against adversarial perturbations. Our solution is built on the manifold hypothesis.

We define a robust classifier on the manifold as $\mathbf{h}_R : \mathbb{R}^m \rightarrow \mathcal{Y}$, which yields a class prediction $\mathbf{y}_{\text{pred}} = \mathbf{h}_R(\mathbf{z})$ given a latent vector $\mathbf{z} \in \mathbb{R}^m$.

Definition 2. (*Robust classifier on the manifold \mathcal{M}*) A robust classifier \mathbf{h}_R on the manifold \mathcal{M} satisfies the following condition: for all $\mathbf{z} \in \mathbb{R}^m$, $\mathbf{h}_R(\mathbf{z}) = (\mathbf{G}_R \circ \mathbf{f}^\dagger)(\mathbf{z})$.

A classifier on the manifold \mathcal{M} is a robust classifier if its predictions are perfectly correlated with the semantic interpretations of the decoder's outputs. Since both \mathbf{h}_R and \mathbf{f}^\dagger take the same low-dimensional vector \mathbf{z} , it is easier to correlate them than achieving adversarial robustness for an encoder \mathbf{f} with inputs from high-dimensional image space. Many studies have shown that high-dimensional inputs are more vulnerable to adversarial attacks; therefore, if the manifold dimension is lower, models applied on the manifold should be more robust.

Objective of this work is to provide sufficient conditions for $\mathbf{h}_R \circ \mathbf{f}$ to be consistent with \mathbf{G}_R against adversarial perturbation δ_{adv} with $\|\delta_{\text{adv}}\|_p \leq \tau/3$. The encoder model \mathbf{f} takes high dimensional inputs and is vulnerable to adversarial examples. In below, we start with description of our assumptions and the triangle inequality of the ℓ_p -norm, then we lay out the sufficient conditions for adversarial robustness.

Assumptions: We assume the adversarial perturbation δ_{adv} and the purified signal ϵ_{pfy} are ℓ_p -bounded where $\|\delta_{\text{adv}}\|_p \leq \tau/3$ and $\|\epsilon_{\text{pfy}}\|_p \leq \tau/3$. Another assumption is that for every point $(\mathbf{x}, \mathbf{y}) \in \mathcal{D}_{XY}$, we have $\|\mathbf{x} - (\mathbf{f}^\dagger \circ \mathbf{f})(\mathbf{x})\|_p \leq \tau/3$.

Triangle Inequality of the ℓ_p -norm: The ℓ_p -norm of a vector $\mathbf{a} = [a_1, \dots, a_n]^\top$ is defined as $\|\mathbf{a}\|_p = (\sum_{k=1}^n |a_k|^p)^{1/p}$ for $1 \leq p < \infty$. We follow the literature to define the ℓ_∞ -norm of the vector as $\|\mathbf{a}\|_\infty = \max\{|a_1|, \dots, |a_n|\}$ and the ℓ_0 -norm of the vector as number of non-zero elements. Considering another vector $\mathbf{b} \in \mathbb{R}^n$, based on the Minkowski inequality, for $1 \leq p < \infty$, we have $\|\mathbf{a} + \mathbf{b}\|_p \leq \|\mathbf{a}\|_p + \|\mathbf{b}\|_p$. For the ℓ_∞ -norm, we know $\|\mathbf{a} + \mathbf{b}\|_\infty = \max\{|a_1 + b_1|, \dots, |a_n + b_n|\} \leq \max\{|a_1| + |b_1|, \dots, |a_n| + |b_n|\} \leq \|\mathbf{a}\|_\infty + \|\mathbf{b}\|_\infty$. Follow the similar proof, we also have $\|\mathbf{a} + \mathbf{b}\|_0 \leq \|\mathbf{a}\|_0 + \|\mathbf{b}\|_0$. Thus, for common p values $\{0, 2, \infty\}$, we have $\|\mathbf{a} + \mathbf{b}\|_p \leq \|\mathbf{a}\|_p + \|\mathbf{b}\|_p$. We focus on these p values in following analysis (we do not consider $0 < p < 1$ since these are not common p values).

Lemma 1. *If an adversarial example \mathbf{x}_{adv} causes $(\mathbf{h}_R \circ \mathbf{f})(\mathbf{x}_{\text{adv}}) \neq \mathbf{G}_R(\mathbf{x}_{\text{adv}})$, then we have $\|\mathbf{x}_{\text{adv}} - (\mathbf{f}^\dagger \circ \mathbf{f})(\mathbf{x}_{\text{adv}})\|_p > 2\tau/3$.*

Proof. We can use proof by contradiction. Assuming \mathbf{x}_{adv} is an adversarial example which causes $(\mathbf{h}_R \circ \mathbf{f})(\mathbf{x}_{\text{adv}}) \neq \mathbf{G}_R(\mathbf{x}_{\text{adv}})$ and $\|\mathbf{x}_{\text{adv}} - (\mathbf{f}^\dagger \circ \mathbf{f})(\mathbf{x}_{\text{adv}})\|_p \leq 2\tau/3$.

Given any vector $\xi \in \mathbb{R}^n$ which satisfies $\|\xi\|_p \leq 2\tau/3$, we have $\|(\mathbf{x}_{\text{adv}} + \xi) - \mathbf{x}\|_p = \|(\mathbf{x} + \delta_{\text{adv}} + \xi) - \mathbf{x}\|_p = \|\delta_{\text{adv}} + \xi\|_p \leq \|\delta_{\text{adv}}\|_p + \|\xi\|_p \leq \tau/3 + 2\tau/3 = \tau$. It implies that given an adversarial example \mathbf{x}_{adv} , for all $\hat{\mathbf{x}} \in \mathbb{R}^n$ and $\|\hat{\mathbf{x}} - \mathbf{x}_{\text{adv}}\|_p \leq 2\tau/3$, we have $\mathbf{G}_R(\mathbf{x}_{\text{adv}}) = \mathbf{G}_R(\hat{\mathbf{x}}) = \mathbf{G}_R(\mathbf{x})$.

If $\|\mathbf{x}_{\text{adv}} - (\mathbf{f}^\dagger \circ \mathbf{f})(\mathbf{x}_{\text{adv}})\|_p \leq 2\tau/3$, we have $\mathbf{G}_R(\mathbf{x}_{\text{adv}}) = (\mathbf{G}_R \circ \mathbf{f}^\dagger \circ \mathbf{f})(\mathbf{x}_{\text{adv}})$. Based on the definition of \mathbf{h}_R , we have $(\mathbf{h}_R \circ \mathbf{f})(\mathbf{x}_{\text{adv}}) = (\mathbf{G}_R \circ \mathbf{f}^\dagger \circ \mathbf{f})(\mathbf{x}_{\text{adv}})$.

Since $(\mathbf{h}_R \circ \mathbf{f})(\mathbf{x}_{\text{adv}}) \neq \mathbf{G}_R(\mathbf{x}_{\text{adv}})$, the assumption is violated. Therefore, $\|\mathbf{x}_{\text{adv}} - (\mathbf{f}^\dagger \circ \mathbf{f})(\mathbf{x}_{\text{adv}})\|_p > 2\tau/3$ \square

Theorem 1. *If a purified signal $\epsilon_{\text{pfy}} \in \mathbb{R}^n$ ensures that $\|(\mathbf{x}_{\text{adv}} + \epsilon_{\text{pfy}}) - (\mathbf{f}^\dagger \circ \mathbf{f})(\mathbf{x}_{\text{adv}} + \epsilon_{\text{pfy}})\|_p \leq \tau/3$, then $(\mathbf{h}_R \circ \mathbf{f})(\mathbf{x}_{\text{adv}} + \epsilon_{\text{pfy}}) = \mathbf{G}_R(\mathbf{x})$.*

Proof. Given any vector $\zeta \in \mathbb{R}^n$ with $\|\zeta\|_p \leq \tau/3$, we have $\|(\mathbf{x}_{\text{pfy}} + \zeta) - \mathbf{x}\|_p = \|(\mathbf{x} + \delta_{\text{adv}} + \epsilon_{\text{pfy}} + \zeta) - \mathbf{x}\|_p = \|\delta_{\text{adv}} + \epsilon_{\text{pfy}} + \zeta\|_p \leq \|\delta_{\text{adv}}\|_p + \|\epsilon_{\text{pfy}}\|_p + \|\zeta\|_p \leq \tau$. It implies that given an purified example \mathbf{x}_{pfy} , for all $\hat{\mathbf{x}} \in \mathbb{R}^n$ and $\|\hat{\mathbf{x}} - \mathbf{x}_{\text{pfy}}\|_p \leq \tau/3$, we have $\mathbf{G}_R(\mathbf{x}_{\text{pfy}}) = \mathbf{G}_R(\hat{\mathbf{x}}) = \mathbf{G}_R(\mathbf{x})$.

Thus, $\|(\mathbf{x}_{\text{adv}} + \epsilon_{\text{pfy}}) - (\mathbf{f}^\dagger \circ \mathbf{f})(\mathbf{x}_{\text{adv}} + \epsilon_{\text{pfy}})\|_p \leq \tau/3$ is a sufficient condition for $\mathbf{G}_R(\mathbf{x}_{\text{adv}} + \epsilon_{\text{pfy}}) = (\mathbf{G}_R \circ \mathbf{f}^\dagger \circ \mathbf{f})(\mathbf{x}_{\text{adv}} + \epsilon_{\text{pfy}})$. Based on the definition of \mathbf{h}_R , we have $(\mathbf{h}_R \circ \mathbf{f})(\mathbf{x}_{\text{adv}} + \epsilon_{\text{pfy}}) = (\mathbf{G}_R \circ \mathbf{f}^\dagger \circ \mathbf{f})(\mathbf{x}_{\text{adv}} + \epsilon_{\text{pfy}})$. Then we have $(\mathbf{h}_R \circ \mathbf{f})(\mathbf{x}_{\text{adv}} + \epsilon_{\text{pfy}}) = \mathbf{G}_R(\mathbf{x}_{\text{adv}} + \epsilon_{\text{pfy}}) = \mathbf{G}_R(\mathbf{x})$. \square

Existence of the solution: If $\epsilon_{\text{pfy}} = -\delta_{\text{adv}}$, based on the assumption that \mathbf{f} and \mathbf{f}^\dagger are approximate inverse for $(\mathbf{x}, \mathbf{y}) \in \mathcal{D}_{XY}$, we have $\|(\mathbf{x}_{\text{adv}} + \epsilon_{\text{pfy}}) - (\mathbf{f}^\dagger \circ \mathbf{f})(\mathbf{x}_{\text{adv}} + \epsilon_{\text{pfy}})\|_p \leq \tau/3$. Thus, the set of feasible solutions for ϵ_{pfy} is non-empty.

Generalization to other distance metrics: Our proof rely on triangle inequality; thus, it can be extent to other distance metrics.

By now, we define the sufficient conditions for the $\mathbf{h}_R \circ \mathbf{f}$ to be consistent with the robust classifier \mathbf{G}_R against adversarial attacks. Instead of constructing a model which is robust to high-dimensional adversarial perturbations, we aim to enforce the correlations between the classifier on the manifold and the decoder on the manifold. We summarize key assumptions of our formulation: 1) The encoding-decoding process performs well on natural images; 2) Adding a vector to an adversarial example does not change the semantic interpretation; 3) A classifier \mathbf{h}_R on the manifold is perfectly correlated with the decoder.

The first assumption is realistic and standard autoencoders should satisfy it. For the second assumption, if ℓ_p -norm of the vector is small, the semantic interpretation should be the same. For the last assumption, it is difficult to obtain a perfectly robust classifier on the manifold despite the dimension of the manifold being much lower. Thus, we need to relax the last assumption. The Bayesian method provides a mathematical grounded framework to quantify the reliability of a prediction. Therefore, we assume that predictions made with high posterior density $p_\theta(\mathbf{z}|\mathbf{x}) = p_\theta(\mathbf{x}|\mathbf{z})p_\theta(\mathbf{z})/p_\theta(\mathbf{x})$, where θ parametrizes the distribution, are similar to predictions from a robust classifier on the manifold. However, the calculation of $p_\theta(\mathbf{x})$ is intractable, an approximation of $p_\theta(\mathbf{z}|\mathbf{x})$ is needed. Variational inference uses different parameters ϕ to approximate the posterior $p_\theta(\mathbf{z}|\mathbf{x})$ as $q_\phi(\mathbf{z}|\mathbf{x})$.

The objective of estimating parameters ϕ is through maximizing the evidence lower bound (ELBO) that is

$$\log p_{\theta}(\mathbf{x}) \geq \underbrace{\mathbb{E}_{\mathbf{z} \sim q_{\phi}(\mathbf{z}|\mathbf{x})} [\log p_{\theta}(\mathbf{x}|\mathbf{z})] - D_{\text{KL}}[q_{\phi}(\mathbf{z}|\mathbf{x}) \| p(\mathbf{z})]}_{\text{ELBO}}. \quad (1)$$

3.3. Jointly Train the ELBO with Classification

In this section, we validate our developed framework with variational inference. We assume that the latent vector \mathbf{z} contains information associated with the class label of the input image \mathbf{x} . We define the one-hot encoded image label vector as $\mathbf{y} = [y_1, y_2, \dots, y_c]^T$ where c is the number of classes and $y_i = 1$ if the image label is i otherwise it will be zero. We define a classification function parametrized by ψ as $\mathbf{h}_{\psi}(\mathbf{z}) = [h_1(\mathbf{z}), h_2(\mathbf{z}), \dots, h_c(\mathbf{z})]^T$. The cross-entropy classification loss is defined as $-\mathbb{E}_{\mathbf{z} \sim q_{\phi}(\mathbf{z}|\mathbf{x})} [\mathbf{y}^T \log \mathbf{h}_{\psi}(\mathbf{z})]$ which we assume to be smaller than a threshold T . The objective of the optimization can then be represented as

$$\max_{\theta, \phi} \mathbb{E}_{\mathbf{z} \sim q_{\phi}(\mathbf{z}|\mathbf{x})} [\log p_{\theta}(\mathbf{x}|\mathbf{z})] - D_{\text{KL}}[q_{\phi}(\mathbf{z}|\mathbf{x}) \| p(\mathbf{z})], \quad (2)$$

$$\text{s.t. } -\mathbb{E}_{\mathbf{z} \sim q_{\phi}(\mathbf{z}|\mathbf{x})} [\mathbf{y}^T \log \mathbf{h}_{\psi}(\mathbf{z})] \leq T. \quad (3)$$

We use a Lagrange multiplier with KKT conditions to optimize this objective as

$$\max_{\theta, \phi, \psi} \text{ELBO} + \lambda \mathbb{E}_{\mathbf{z} \sim q_{\phi}(\mathbf{z}|\mathbf{x})} [\mathbf{y}^T \log \mathbf{h}_{\psi}(\mathbf{z})], \quad (4)$$

where λ is a trade-off term that balances the ELBO and the classification loss.

We follow Kingma et al. [13] to define the prior $p(\mathbf{z})$ and the posterior $q(\mathbf{z}|\mathbf{x})$ by both using a normal distribution with diagonal covariance. Given an input vector \mathbf{x} , an inference model is used to model the posterior distribution $q(\mathbf{z}|\mathbf{x})$ which is parametrized by ϕ . The model outputs the mean vector as $\boldsymbol{\mu}_{\phi}(\mathbf{x}) = [\mu_1(\mathbf{x}), \mu_2(\mathbf{x}), \dots, \mu_J(\mathbf{x})]^T$ and the diagonal covariance as $\boldsymbol{\sigma}_{\phi}^2(\mathbf{x}) = [\sigma_1^2(\mathbf{x}), \sigma_2^2(\mathbf{x}), \dots, \sigma_J^2(\mathbf{x})]^T$. Given two Gaussian distributions $q_{\phi}(\mathbf{z}|\mathbf{x}) = \mathcal{N}(\boldsymbol{\mu}_{\phi}(\mathbf{x}), \text{diag}(\boldsymbol{\sigma}_{\phi}^2(\mathbf{x})))$ and $p(\mathbf{z}) = \mathcal{N}(0, I)$, the KL divergence can be calculated in closed form as $D_{\text{KL}}[q_{\phi}(\mathbf{z}|\mathbf{x}) \| p(\mathbf{z})] = -0.5 \sum_{j=1}^J (1 + \log((\sigma_j(\mathbf{x}))^2) - (\mu_j(\mathbf{x}))^2 - (\sigma_j(\mathbf{x}))^2)$.

We define $p_{\theta}(\mathbf{x}|\mathbf{z}) = (1/\beta) \exp(-\|\mathbf{x} - f_{\theta}^{\dagger}(\mathbf{z})\|_2^2/\gamma)$, where γ controls the variance, β is a normalization factor and f_{θ}^{\dagger} is a decoder function, parametrized by θ , which maps data from the latent space to the image space. $\mathbb{E}_{\mathbf{z} \sim q_{\phi}(\mathbf{z}|\mathbf{x})} [\log p_{\theta}(\mathbf{x}|\mathbf{z})] = -(1/\gamma) \mathbb{E}_{\mathbf{z} \sim q_{\phi}(\mathbf{z}|\mathbf{x})} [\|\mathbf{x} - f_{\theta}^{\dagger}(\mathbf{z})\|_2^2] - \log \beta$ is the negative weighted reconstruction error. An example network described by Eq. (4) can be found in Figure 1(a). The architecture is similar to the architecture presented in Bhushan et al. [2].

3.4. Adversarial Attack and Test-Time Defense with Variational Inference

During inference time, attackers can create adversarial perturbations on the classification head to cause prediction failures. An attack objective could maximize the cross-entropy loss as

$$\boldsymbol{\delta}_{\text{adv}} = \arg \max_{\boldsymbol{\delta} \in \mathcal{C}_{\text{adv}}} -\mathbb{E}_{\mathbf{z} \sim q_{\phi}(\mathbf{z}|\mathbf{x}+\boldsymbol{\delta})} [\mathbf{y}^T \log \mathbf{h}_{\psi}(\mathbf{z})], \quad (5)$$

where \mathcal{C}_{adv} is the set of feasible solutions for adversarial perturbations. In this case, $\boldsymbol{\delta}$ is ℓ_p -bounded by a threshold value as $\|\boldsymbol{\delta}\|_p \leq \delta_{\text{th}}$ and $\mathbf{x}_{\text{adv}} = \mathbf{x} + \boldsymbol{\delta} \in [0, 1]^n$.

We observe that adversarial attacks on the classification head $\mathbf{h}_{\psi}(\mathbf{z})$ can change the reconstructions from the decoder as well as increase the negative ELBO as shown in Figure 1(c) and Figure 2. These phenomena indicate that the classification head and the decoder are strongly correlated. Therefore, based on our framework, to defend against adversarial attacks, we can obtain purified signals that project points to regions with higher posterior density $q_{\phi}(\mathbf{z}|\mathbf{x})$ and lower reconstruction loss.

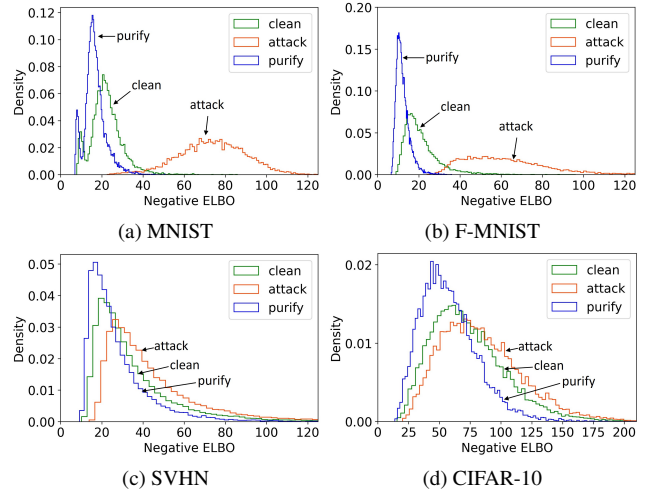


Figure 2. The negative ELBO of (a) MNIST [16], (b) Fashion-MNIST [36], (c) SVHN [21] and (d) CIFAR-10 [15] on clean, adversarial and purified images. Adversarial attacks make the ELBO lower (negative ELBO higher) while our test-time defense reverses the shifts. Compared with MNIST and Fashion-MNIST, SVHN and CIFAR-10 have more diverse backgrounds; thus, the ELBO shifts are less obvious but still observable.

Since attack perturbations are unknown, we need to estimate the purified signal with a ℓ_{∞} -norm smaller than a threshold value ϵ_{th} in order to avoid changing the semantic interpretation of the image. The ELBO consists of reconstruction loss as well as KL divergence, and it can estimate the posterior $q_{\phi}(\mathbf{z}|\mathbf{x})$. Therefore, we present a test-time defense method that optimizes the ELBO during test time

in order to purify attacks as shown in the blue curves of Figure 2. The purification signal ϵ_{pfy} is defined as

$$\arg \max_{\epsilon \in \mathcal{C}_{\text{pfy}}} \mathbb{E}_{\mathbf{z} \sim \hat{q}_{\phi}(\mathbf{z})} [\log p_{\theta}(\mathbf{x}_{\text{adv}} + \epsilon | \mathbf{z})] - D_{\text{KL}}[\hat{q}_{\phi}(\mathbf{z}) \| p(\mathbf{z})], \quad (6)$$

where $\hat{q}_{\phi}(\mathbf{z}) = q_{\phi}(\mathbf{z} | \mathbf{x}_{\text{adv}} + \epsilon)$ and \mathcal{C}_{pfy} is the set of feasible solutions for purification. In this case, $\|\epsilon\|_{\infty} \leq \epsilon_{\text{th}}$ and $\mathbf{x}_{\text{pfy}} = \mathbf{x}_{\text{adv}} + \epsilon \in [0, 1]^n$.

Generating purified signals is similar to generating adversarial perturbations. The only difference is the objective. We define α as the learning rate and $\text{Proj}_{\mathcal{S}}$ as the projection operator which projects a point back to a feasible region if it is out of that region. We use a clipping function as the projection operator, which ensures that $\|\mathbf{x}_{\text{pfy}} - \mathbf{x}\|_{\infty} = \|\epsilon_{\text{pfy}}\|_{\infty} \leq \epsilon_{\text{th}}$ and $\mathbf{x}_{\text{pfy}} = \mathbf{x} + \epsilon_{\text{pfy}} \in [0, 1]^n$, where \mathbf{x} is the input (adversarial) images and ϵ_{th} is the budget for purification which should be small to keep the semantic interpretation of the image. We define $\mathcal{F}(\mathbf{x}; \theta, \phi) = \mathbb{E}_{\mathbf{z} \sim q_{\phi}(\mathbf{z} | \mathbf{x})} [\log p_{\theta}(\mathbf{x} | \mathbf{z})] - D_{\text{KL}}[q_{\phi}(\mathbf{z} | \mathbf{x}) \| p(\mathbf{z})]$. An iterative optimization process given an adversarial example \mathbf{x}_{adv} is

$$\epsilon^{t+1} = \text{Proj}_{\mathcal{S}}(\epsilon^t + \alpha \text{sgn}(\nabla_{\epsilon^t} \mathcal{F}(\mathbf{x}_{\text{adv}} + \epsilon^t; \theta, \phi))), \quad (7)$$

where the element-wise sign function $\text{sgn}(x) = x/|x|$ if x is not zero otherwise the value will be zero.

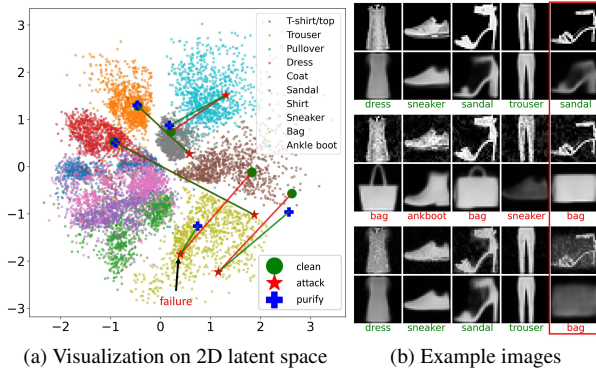


Figure 3. (a) Trajectories of clean (green) - attack (red) - purified (blue) images on a 2D latent space (left). (b) Input images and reconstruction images of samples on the left. The top two rows are input and reconstruction of clean images, the middle two rows are input and reconstruction of adversarial images. The bottom two rows are input and reconstruction of purified images. Text represents predicted classes with green color for correct predictions and red color for incorrect predictions. The red box on the right corresponds to the fail case (purified process fails) on the left.

Purified examples could be obtained by conducting $\mathbf{x}_{\text{pfy}} = \mathbf{x}_{\text{adv}} + \epsilon_{\text{pfy}}$. This is a test-time optimization of the ELBO to project adversarial examples back to regions with high posterior $q(\mathbf{z} | \mathbf{x})$ (a reliable classifier on the manifold) and small reconstruction losses (defend against adversarial attacks). We train a model with a 2-dimensional latent space

on the Fashion-MNIST dataset and show examples of clean, attack and purified trajectories in Figure 3. We observe that adversarial attacks are likely to push latent vectors to abnormal regions which cause abnormal reconstructions. Through test-time optimization of the ELBO, latent vectors can be brought back to their original regions.

If attackers are aware of the existence of the purification process, it is possible to take advantage of this knowledge during the attack generation process. A straightforward formulation for attackers is to perform a multi-objective optimization where a trade-off term λ_a is introduced to balance the classification loss $\mathcal{L}(\mathbf{x}; \mathbf{y}; \theta)$ and the purification objective $\mathcal{F}(\mathbf{x}; \theta, \phi)$. The adversarial perturbation of the multi-objective attack is

$$\delta_{\text{adv}} = \arg \max_{\delta \in \mathcal{C}_{\text{adv}}} \mathcal{L}(\mathbf{x} + \delta; \mathbf{y}; \theta) + \lambda_a \mathcal{F}(\mathbf{x} + \delta; \theta, \phi). \quad (8)$$

Another defense-aware attack is the Backward Pass Differentiable Approximation (BPDA) attack [1]. Consider the purification process as a function $\mathbf{x}_{\text{pfy}} = \mathbf{F}(\mathbf{x})$ and a classifier as $\mathbf{y} = \mathbf{G}(\mathbf{x}_{\text{pfy}}) = (\mathbf{G} \circ \mathbf{F})(\mathbf{x})$. To craft an adversarial example, attackers need the gradient $\nabla_{\hat{\mathbf{x}}} \mathbf{G}(\mathbf{F}(\hat{\mathbf{x}}))|_{\hat{\mathbf{x}}=\mathbf{x}}$; however, it is often difficult to calculate the gradient of the purification process. The BPDA attack uses the straight-through estimator $\nabla_{\hat{\mathbf{x}}} \mathbf{F}(\hat{\mathbf{x}}) \approx \nabla_{\hat{\mathbf{x}}} \hat{\mathbf{x}} = 1$ to approximate the gradient. The gradient can then be approximated as $\nabla_{\hat{\mathbf{x}}} \mathbf{G}(\mathbf{F}(\hat{\mathbf{x}}))|_{\hat{\mathbf{x}}=\mathbf{x}} \approx \nabla_{\hat{\mathbf{x}}} \mathbf{G}(\hat{\mathbf{x}})|_{\hat{\mathbf{x}}=\mathbf{F}(\mathbf{x})}$. Many adversarial purification methods have been shown to be vulnerable to the BPDA attack. In the next section, we show that even if attackers are aware of the test-time defense, our approach can still achieve effective adversarial robustness.

4. Experiments

Implementation details and experiment results are provided in this section. We evaluate our method on MNIST [16], Fashion-MNIST [36], SVHN [21] and CIFAR-10 [15].

4.1. Model Architectures and Hyperparameters

We use several residual blocks [9] to construct the encoder (4 residual blocks) and decoder (6 residual blocks). We set convolution kernel size to 3×3 and use max pooling and upsampling to reduce and increase hidden layer dimensions respectively. We use 64 feature maps in each residual block for MNIST and Fashion-MNIST, 128 for SVHN, and 256 for CIFAR-10. A linear classification head is added on top of the latent vector \mathbf{z} , which is optimized by using the cross-entropy loss with the ground truth class labels. We set the weight of the classification loss to 8 ($\lambda = 8$ in Eq. (4)) and define $\log p(\mathbf{x} | \mathbf{z})$ as the reconstruction loss ($\gamma = 1$). During the inference, we use mean values of the encoder's outputs to replace the sampling steps of VAE models. We also evaluate our method with larger encoder models such as ResNet-50 [9] (standard training) and PreActResNet-18 [25]

(adversarial training). For the adversarially trained model, we freeze the pretrained encoder and train the decoder only. See the appendix for model architectures and training details.

4.2. Adversarial Attacks

We evaluate our method on standard adversarial attacks and defense-aware attacks (multi-objective and BPDA). All attacks are untargeted. For the former, attackers only attack the classification head of the model as shown in Eq. (5). We use Foolbox [24] to generate the FGSM (ℓ_∞) attack [7], the PGD (ℓ_∞) attack [19] and the C&W (ℓ_2) attack [3]. We use the attack generation method in Croce et al. [5] for the AutoAttack (ℓ_∞, ℓ_2), Torchattacks [12] for the defense-aware attacks, specifically the BPDA-PGD (ℓ_∞) and BPDA-APGD (ℓ_∞) attacks [1]. We use PGD (ℓ_∞) for the multi-objective attack.

Specifically, for MNIST and Fashion-MNIST, we set the budget of ℓ_∞ attacks to 50/255 and the budget of ℓ_2 attacks to 3. The PGD (ℓ_∞) attack is conducted in 200 iterations with step size 2/255. For the BPDA attack, we use 100 iterations with step size 2/255. For SVHN and CIFAR-10, we set the budget of ℓ_∞ attacks to 8/255 and the budget of ℓ_2 attacks to 0.5. We run 100 iterations with step size 2/255 for the PGD (ℓ_∞) attack and 50 iterations with step size 2/255 for the BPDA attack.

4.3. Test-Time Defense

Key hyperparameters and experimental details are provided below, and only the ℓ_∞ -bounded purification is considered in this work. We initialize the purified signal ϵ_{pfy} by sampling from an uniform distribution $\mathcal{U}_{[-\epsilon_{\text{th}}, \epsilon_{\text{th}}]}$ where ϵ_{th} is the budget of purification. We run test-time defense 16 times with different initialization and select the run with the best purification score (the reconstruction loss or the ELBO) as our final purified signal. Step size α alternates between 1/255 and 2/255 for each run.

For MNIST and Fashion-MNIST, we set the budget (ϵ_{th}) of ℓ_∞ -purification to 50/255 with 96 purification iterations. For SVHN and CIFAR-10, we set the budget (ϵ_{th}) of ℓ_∞ -purification to 8/255 with 32 purification iterations.

Despite the aforementioned hyperparameters, we also observe from the experiments that our proposed approach works on other hyperparameter settings as shown in Figure 7. **Baselines:** We perform experiments by using the standard autoencoders (only trained with the reconstruction loss) which architectures are similar to VAE models. We use VAE-Classifier (VAE-CLF) and Standard-AE-Classifier (ST-AE-CLF) to distinguish these two architectures. One should note that the classifiers of the Standard-AE-Classifier models may not have strong correlations with their decoders due to the lack of semantic correlation as illustrated in Figure 1.

Objectives of Our Test-Time Defense: In this work, we jointly train the autoencoder and the classifier by using the re-

construction loss and the ELBO respectively. The Standard-AE-Classifier models can only minimize the reconstruction loss during test time while the VAE-Classifier models can optimize both the reconstruction loss and the ELBO. We use TTD (REC) to represent the test-time optimization on the reconstruction loss and TTD (ELBO) for the test-time optimization on the ELBO.

4.4. Experiment Results

We start with the evaluation of the standard adversarial attacks, where attackers only attack the classification heads. Then, we evaluate our method on the defense-aware attacks including multi-objective attacks and the BPDA attacks. We also conduct an ablation study for the effects of different hyperparameters on our test-time defense.

Standard Adversarial Attacks: For the standard adversarial attacks, only the classification heads are attacked. We observe that, for MNIST, Fashion-MNIST and SVHN, adversarial attacks on the classification heads of the VAE-Classifier models create abnormal reconstructed images while this is not applied to the Standard-AE-Classifier. This indicates that the classification heads and the decoders of the VAE-Classifier models are strongly correlated. Figure 4 shows various sample predictions and reconstructions on clean, attack and purified images by using the VAE-Classifier models. For clean images, the VAE-Classifier models achieve qualified reconstruction images and predictions. With the attacks, abnormal reconstructions are correlated with abnormal predictions from the classification heads of the VAE-Classifier models. If the predicted class of an adversarial example is 2, the digit on the reconstructed image may look like 2. With our test-time defense (ELBO), both the reconstructions and the predictions are normal and strongly correlated.

Figure 5 shows various sample predictions and reconstructions of the Standard-AE-Classifier models and the VAE-Classifier models on CIFAR-10. The results are slightly different from those on MNIST, Fashion-MNIST and SVHN: in Figure 5, the reconstructed images from the VAE-Classifier models are blur. Changing semantic interpretations in the reconstructions during attacks is less frequent for CIFAR-10 (compared with MNIST, Fashion-MNIST and SVHN), but we still observe many samples and show them in Figure 5. Although the VAE-Classifier models on CIFAR-10 fail to completely satisfy the assumptions of our framework (that is high correlations between decoders and classifiers and low reconstruction errors), our test-time defense still achieves competitive adversarial robustness.

For the classification task, we use small ResNet backbones for the Standard-AE-Classifier models and the VAE-Classifier models. The classification accuracy with test-time defense (optimized on both the reconstruction loss and the ELBO) is provided in Tables 1-2. We observe that the optimization on the single reconstruction loss during test time is

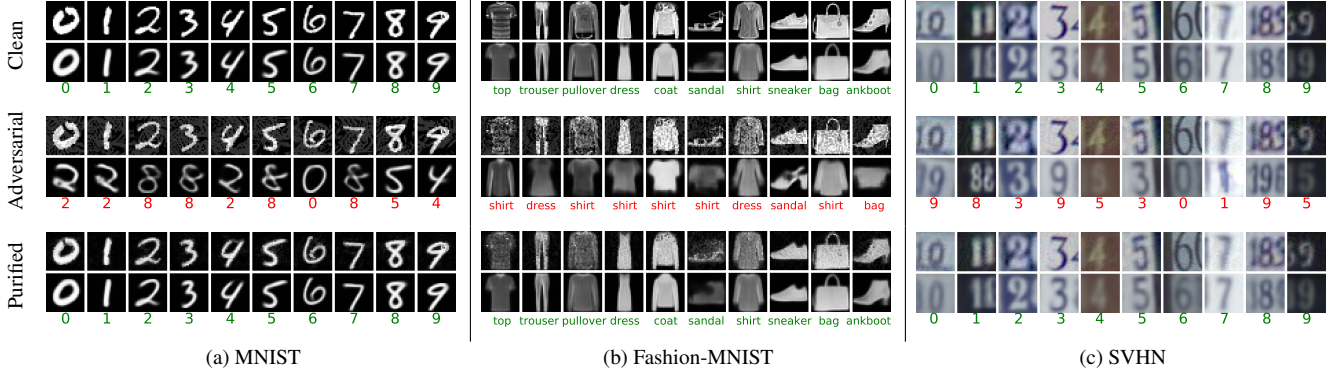


Figure 4. Class prediction by using the VAE-Classifier models on clean, adversarial and purified samples of MNIST, Fashion-MNIST and SVHN. The top two rows are input and reconstruction of clean images, the middle two rows are input and reconstruction of adversarial images. The bottom two rows are input and reconstruction of purified images. Text represents the predicted classes with **green** color for correct predictions and **red** color for incorrect predictions. Since predictions and reconstructions are correlated with the VAE-Classifier models, our test-time defenses are effective against adversarial attacks.

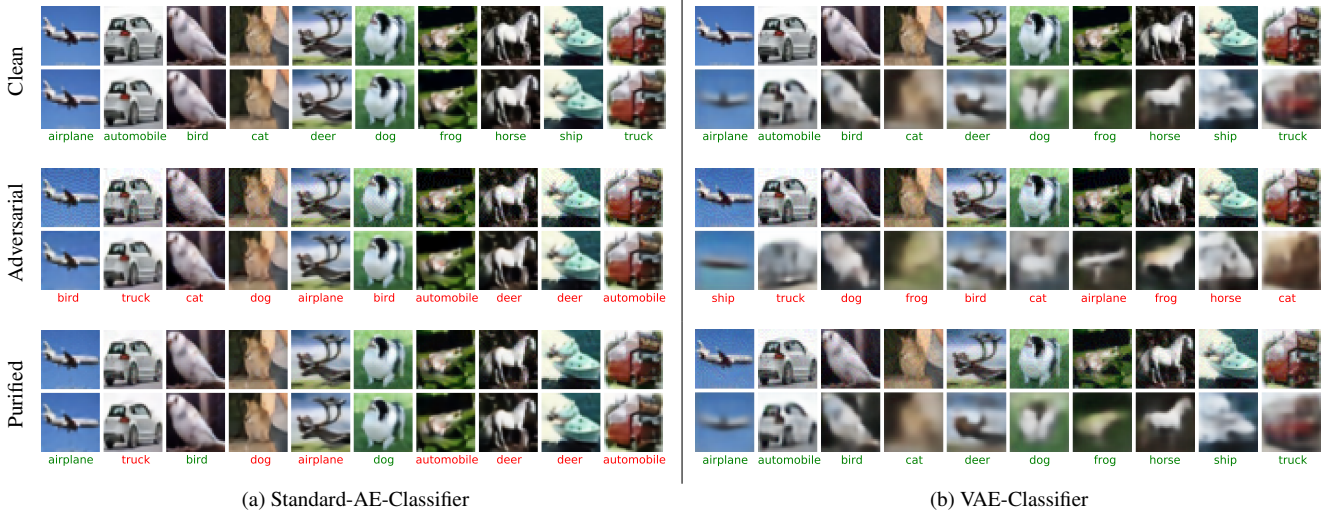


Figure 5. Class prediction on clean, adversarial and purified samples of CIFAR-10. The notations are the same as those in Figure 4. The left column uses the Standard-AE-Classifier model and the right column uses the VAE-Classifier model. Compared with models trained on other datasets, the VAE-Classifier model trained on CIFAR-10 produces blur reconstruction images, but our test-time defense can still achieve competitive performance.

less effective than the ELBO. Table 3 shows the CIFAR-10 classification accuracy with our test-time defense method using larger backbones such as ResNet-50 (standard training) and PreActResNet-18 (adversarial training). With our test-time defense, the robust accuracy of the ResNet-50 model on CIFAR-10 can increase by more than 50%. Furthermore, our method can also be applied to adversarially trained models to further increase the robust accuracy. We compare our method with other works in Tables 4-5.

Multi-Objective Attacks: We perform the multi-objective attack experiments on SVHN as well as CIFAR-10 and provide the accuracy versus trade-off term λ_a of Eq. (8) in Fig-

ure 6. We observe that the accuracy of adversarial examples increases as the trade-off term increase. In the meantime, the increase of the trade-off term has no significant degradation on our test-time defense. Therefore, our test-time defense method is robust to multi-objective attacks.

Backward Pass Differentiable Approximation (BPDA): We use PGD and APGD to optimize the objective of the BPDA attack. We highlight the minimum classification accuracy from our experiments in Tables 1-3. We observe that although the BPDA attack is the strongest compared with the standard adversarial attacks and multi-objective attacks, our test-time defense still achieves desirable adversarial ro-

bustness. In our experiments, models with larger backbones are more robust to the BPDA attack.

Table 1. *Classification accuracy on MNIST and Fashion-MNIST. We set $\ell_\infty = 50/255$ and $\ell_2 = 3$.*

Dataset	Method	Clean	FGSM	PGD	AA- ℓ_∞	AA- ℓ_2	BPDA
MNIST	ST-AE-CLF	99.26	44.43	0.00	0.00	0.00	-
	+TTD (REC)	99.21	89.60	90.80	91.21	20.80	77.41
	VAE-CLF	99.33	49.20	2.21	0.00	0.00	-
	+TTD (REC)	99.27	90.24	67.60	53.81	67.09	68.03
	+TTD (ELBO)	99.17	93.31	86.33	85.20	81.36	83.08
F-MNIST	ST-AE-CLF	92.24	10.05	0.00	0.00	0.00	-
	+TTD (REC)	88.24	28.72	17.83	14.57	10.91	3.65
	VAE-CLF	92.33	36.96	0.00	0.00	0.00	-
	+TTD (REC)	86.03	67.31	69.75	66.77	68.94	49.82
	+TTD (ELBO)	84.79	71.09	73.44	71.48	73.64	60.24

Table 2. *Classification accuracy on SVHN and CIFAR-10. We set $\ell_\infty = 8/255$ and $\ell_2 = 0.5$.*

Dataset	Method	Clean	FGSM	PGD	AA- ℓ_∞	AA- ℓ_2	BPDA
SVHN	ST-AE-CLF	94.00	8.88	0.00	0.00	1.67	-
	+TTD (REC)	93.03	40.10	40.83	44.82	59.93	7.65
	VAE-CLF	95.27	70.24	16.01	0.33	6.61	-
	+TTD (REC)	90.66	77.03	72.44	73.92	79.15	66.68
	+TTD (ELBO)	86.29	75.40	72.72	73.47	76.21	64.70
CIFAR-10	ST-AE-CLF	90.96	6.42	0.00	0.00	0.98	-
	+TTD (REC)	87.80	19.36	11.65	13.74	44.57	0.70
	VAE-CLF	91.82	54.55	17.82	0.05	2.36	-
	+TTD (REC)	78.51	57.24	51.20	51.63	59.35	43.02
	+TTD (ELBO)	77.97	59.51	57.21	58.78	63.38	47.43

Table 3. *Classification accuracy of VAE-Classifier models with ResNet-50 and adversarially trained PreActResNet-18 on CIFAR-10. We set $\ell_\infty = 8/255$ and $\ell_2 = 0.5$.*

Backbone	Method	Clean	FGSM	PGD	AA- ℓ_∞	AA- ℓ_2	CW- ℓ_2	BPDA
ResNet-50	VAE-CLF	94.82	72.10	23.84	0.04	3.42	20.21	-
	+TTD (ELBO)	85.12	70.83	63.09	63.16	68.21	73.63	57.15
PreAct-ResNet-18	VAE-CLF	87.35	66.38	61.08	58.65	65.67	66.58	-
	+TTD (ELBO)	85.14	65.74	61.98	63.73	70.06	73.85	60.52

Table Notes: “ST-AE”: standard autoencoder; “CLF”: classifier; “TTD”: Test-Time Defense; “REC”: minimization of the reconstruction loss; “ELBO”: minimization of the negative ELBO loss; “F-MNIST”: Fashion-MNIST; “AA”: AutoAttack; “BPDA”: Backward Pass Differentiable Approximation. We evaluate the performance of models on both BPDA-PGD and BPDA-APGD and record the minimum accuracy in the tables. We highlight the numbers of test-time defense from PGD, AutoAttack and BPDA for better comparison. For ResNet-50 trained on CIFAR-10, we also study the impact of random noise and smoothing filter on the defense against AutoAttacks- ℓ_∞ . Adding a uniform noise with the same purification budget achieves 9.55% accuracy. Adding a unit variance Gaussian achieves 12.8% accuracy. Applying a 3*3 average filter achieves 54.04% but 5.32% with BPDA-AutoAttack.

Effects of Hyperparameters: We study the impacts of purification budgets for ϵ_{pfy} , the number of purification iter-

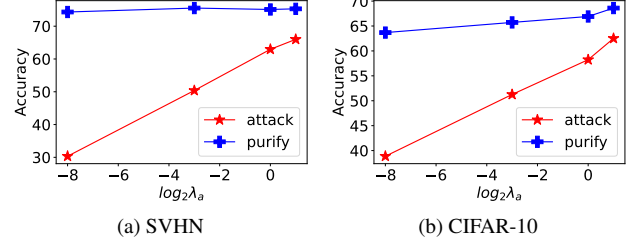


Figure 6. *Classification accuracy with multi-objective attack and test-time defense. As λ_a increases, the classification accuracy of adversarial examples increases, in the meantime, the impacts on our test-time defense are not significant.*

ations and the adversarial perturbation budgets for ϵ_{adv} on clean classification accuracy and adversarial robustness. We use the VAE-Classifier models with small ResNet backbones to perform experiments and show results in Figure 7. Our test-time defense can provide adversarial robustness with various settings of these hyperparameters.

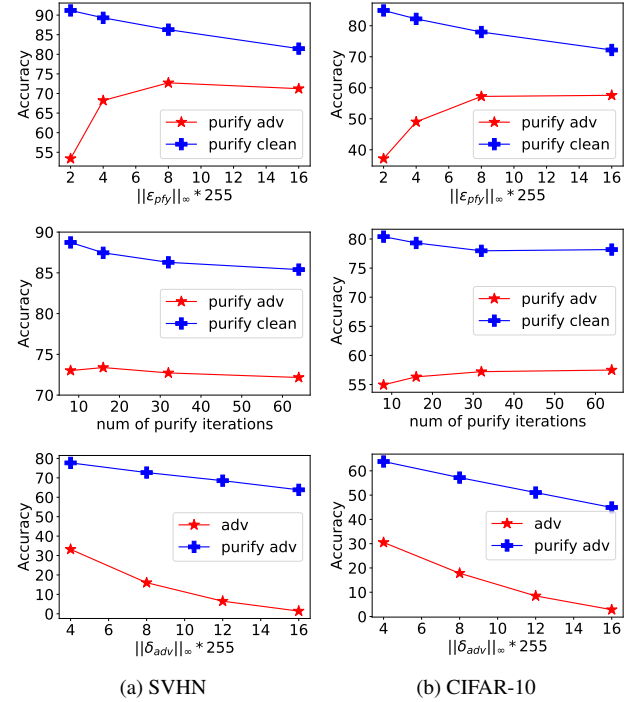


Figure 7. *Effects of hyperparameters on classification. Top: Given adversarial perturbations of $\ell_\infty = 8/255$, the change of accuracy with respect to the ℓ_∞ purification budgets. Middle: Given adversarial perturbations of $\ell_\infty = 8/255$ and a purification budget of $\ell_\infty = 8/255$, the change of accuracy with respect to the number of purification iterations. Bottom: Given a purification budget of $\ell_\infty = 8/255$ and 32 purification iterations, the change of accuracy with respect to ℓ_∞ adversarial perturbation budgets.*

Inference Time: We evaluate our test-time defense on an NVIDIA Tesla P100 GPU. With a batch size of 256 for

Table 4. Benchmark of image classification on SVHN.

Method	FGSM	PGD	APGD	AA- ℓ_∞	BPDA
Mao et al. (Semi-SL*) [20]	-	62.12	-	65.50	-
Rice et al. (PreActResNet-18*) [26]	-	61.00	-	-	-
Rebuffi et al. (Wide-ResNet-28*) [25]	-	-	-	61.09	-
Ours (small ResNet)	75.40	72.72	-	73.47	64.70

Table 5. Benchmark of image classification on CIFAR-10.

Method	FGSM	PGD	APGD	AA- ℓ_∞	BPDA
SOAP (Wide-ResNet-28) [29]	64.83	53.58	-	-	3.70 [4]
PixelDefend (ResNet) [30]	46.00	46.00	-	-	9.00 [1]
Stoc. Security (Wide-ResNet-28) [10]	-	78.91	-	-	54.90
Score-Based (Wide-ResNet-28) [37]	-	85.45	33.70 [4]	-	69.71
Mao et al. (PreActResNet-18) [20]	-	-	-	34.40	-
Mao et al. (Semi-SL*) [20]	-	64.44	-	67.79	58.40 [4]
Madry et al. (Wide-ResNet-34*) [19]	-	-	-	44.04	-
TRADES (Wide-ResNet-34*) [38]	-	-	-	53.08	-
Rebuffi et al. (Wide-ResNet-70*) [25]	-	-	-	66.56	-
Rebuffi et al. (PreActResNet18*) [25]	-	-	-	58.50	-
Ours (ResNet-50)	70.83	63.09	-	63.16	57.15

Table Notes: “*” indicates that adversarially trained model is used. The APGD attack is part of the AutoAttack (AA). Numbers in **bold** are the minimum robust accuracy that can be achieved by the related methods. Our test-time defense method achieves competitive and robust accuracy compared with the others.

a ResNet-50 (CIFAR-10) model, the average run time per batch for 32 purification steps is 17.65s. Our method is implemented in PyTorch.

Limitations: Our method requires an accurate estimation of $p(\mathbf{z}|\mathbf{x})$ for each class. We observe that if the number of training samples for each class is small or the label set is large, the performance of our method could decrease. On CIFAR-100 [15], we train two VAE-Classifer models by using ResNet-50 ($\lambda = 8$ and 16 in Eq. (4)). The classification accuracy without our test-time defense is 68.96% ($\lambda = 8$) and 75.74% ($\lambda = 16$). It drops to 0.05% and 0.06% with the AutoAttack. However, with our test-time defense, the purified accuracy is boosted to 23.01% and 19.48%. Although compared with the high accuracy increase on CIFAR-10, the accuracy increase on CIFAR-100 by using our test-time defense is limited.

5. Conclusion

In this work, we develop a novel framework for adversarial robustness and present a test-time defense method by using variational inference and this framework. Our method combines manifold learning with variational inference. We evaluate the presented test-time defense method through several attacks and show adversarial robustness for non-adversarially trained models. Even if attackers are aware of our test-time defense method, our method can still provide competitive adversarial robustness. Our method is also capable to defend against adversarial attacks related to VAEs or be combined with adversarially trained models to further increase the adversarial robustness.

Acknowledgments

Research is supported by DARPA Geometries of Learning (GoL) program under the agreement No. HR00112290075. The views, opinions, and/or findings expressed are those of the author(s) and should not be interpreted as representing the official views or policies of the Department of Defense or the U.S. government.

References

- [1] Anish Athalye, Nicholas Carlini, and David Wagner. Obfuscated gradients give a false sense of security: Circumventing defenses to adversarial examples. In *International Conference on Machine Learning*, pages 274–283. PMLR, 2018. 5, 6, 9
- [2] Chitresh Bhushan, Zhaoyuan Yang, Nurali Virani, and Naresh Iyer. Variational encoder-based reliable classification. In *2020 IEEE International Conference on Image Processing (ICIP)*, pages 1941–1945. IEEE, 2020. 4
- [3] Nicholas Carlini and David Wagner. Towards evaluating the robustness of neural networks. In *2017 IEEE Symposium on Security and Privacy (SP)*, pages 39–57. IEEE, 2017. 6
- [4] Francesco Croce, Sven Gowal, Thomas Brunner, Evan Shelhamer, Matthias Hein, and A. Taylan Cemgil. Evaluating the adversarial robustness of adaptive test-time defenses. In *ICML*, volume 162 of *Proceedings of Machine Learning Research*, pages 4421–4435. PMLR, 2022. 1, 9
- [5] Francesco Croce and Matthias Hein. Reliable evaluation of adversarial robustness with an ensemble of diverse parameter-free attacks. In *International Conference on Machine Learning*, 2020. 6
- [6] Partha Ghosh, Arpan Losalka, and Michael J Black. Resisting adversarial attacks using Gaussian mixture variational autoencoders. In *AAAI Conference on Artificial Intelligence*, 2019. 2
- [7] Ian J. Goodfellow, Jonathon Shlens, and Christian Szegedy. Explaining and harnessing adversarial examples. In *ICLR*, 2015. 1, 6
- [8] Will Grathwohl, Kuan-Chieh Wang, Jorn-Henrik Jacobsen, David Duvenaud, Mohammad Norouzi, and Kevin Swersky. Your classifier is secretly an energy based model and you should treat it like one. In *International Conference on Learning Representations*, 2020. 2
- [9] Kaiming He, Xiangyu Zhang, Shaoqing Ren, and Jian Sun. Deep residual learning for image recognition. In *IEEE Conference on Computer Vision and Pattern Recognition*, pages 770–778, 2016. 5
- [10] Mitch Hill, Jonathan Mitchell, and Song-Chun Zhu. Stochastic security: Adversarial defense using long-run dynamics of energy-based models. In *International Conference on Learning Representations*, 2021. 2, 9
- [11] Uiwon Hwang, Jaewoo Park, Hyemi Jang, Sungroh Yoon, and Nam Ik Cho. Puvae: A variational autoencoder to purify adversarial examples. In *IEEE Access*, 2019. 2
- [12] Hoki Kim. Torchattacks: A pytorch repository for adversarial attacks. *arXiv preprint arXiv:2010.01950*, 2020. 6

- [13] Diederik P. Kingma and Max Welling. Auto-encoding variational bayes. In *ICLR*, 2014. 2, 4
- [14] Jernej Kos, Ian Fischer, and Dawn Song. Adversarial examples for generative models. In *2018 IEEE Security and Privacy Workshops (SPW)*, pages 36–42. IEEE, 2018. 2
- [15] Alex Krizhevsky and Geoffrey Hinton. Learning multiple layers of features from tiny images. Technical Report 0, University of Toronto, Toronto, Ontario, 2009. 4, 5, 9
- [16] Yann LeCun, Corinna Cortes, and CJ Burges. Mnist handwritten digit database. *ATT Labs [Online]*. Available: <http://yann.lecun.com/exdb/mnist>, 2, 2010. 4, 5
- [17] Xiang Li and Shihao Ji. Defense-VAE: A fast and accurate defense against adversarial attacks. In *Joint European Conference on Machine Learning and Knowledge Discovery in Databases*, 2019. 2
- [18] Weian Lin, Chun Pong Lau, Alexander Levine, Rama Chellappa, and Soheil Feizi. Dual manifold adversarial robustness: Defense against l_p and non- l_p adversarial attacks. In *Advances in Neural Information Processing Systems*, volume 33, pages 3487–3498, 2020. 2
- [19] Aleksander Madry, Aleksandar Makelov, Ludwig Schmidt, Dimitris Tsipras, and Adrian Vladu. Towards deep learning models resistant to adversarial attacks. In *International Conference on Learning Representations*, 2018. 1, 6, 9
- [20] Chengzhi Mao, Mia Chiquier, Hao Wang, Junfeng Yang, and Carl Vondrick. Adversarial attacks are reversible with natural supervision. In *IEEE International Conference on Computer Vision*, pages 661–671, 2021. 2, 9
- [21] Yuval Netzer, Tao Wang, Adam Coates, Alessandro Bissacco, Bo Wu, and Andrew Y Ng. Reading digits in natural images with unsupervised feature learning. In *NIPS Workshop on Deep Learning and Unsupervised Feature Learning*, 2011. 4, 5
- [22] Tianyu Pang, Xiao Yang, Yinpeng Dong, Hang Su, and Jun Zhu. Bag of tricks for adversarial training. In *International Conference on Learning Representations*, 2020. 2
- [23] Kanil Patel, William Beluch, Dan Zhang, Michael Pfeiffer, and Bin Yang. On-manifold adversarial data augmentation improves uncertainty calibration. In *International Conference on Pattern Recognition*, 2020. 2
- [24] Jonas Rauber, Wieland Brendel, and Matthias Bethge. Foolbox: A python toolbox to benchmark the robustness of machine learning models. In *Reliable Machine Learning in the Wild Workshop, 34th International Conference on Machine Learning*, 2017. 6
- [25] Sylvestre-Alvise Rebuffi, Sven Gowal, Dan A Calian, Florian Stimberg, Olivia Wiles, and Timothy Mann. Fixing data augmentation to improve adversarial robustness. *arXiv preprint arXiv:2103.01946*, 2021. 2, 5, 9
- [26] Leslie Rice, Eric Wong, and Zico Kolter. Overfitting in adversarially robust deep learning. In *International Conference on Machine Learning*, pages 8093–8104. PMLR, 2020. 9
- [27] Pouya Samangouei, Maya Kabkab, and Rama Chellappa. Protecting classifiers against adversarial attacks using generative models. In *International Conference on Learning Representations*, 2018. 2
- [28] Yin Shenglin, Zhang Xinglan, and Zuo Liyu. Defending against adversarial attacks using spherical sampling-based variational auto-encoder. In *Neurocomputing*, 2022. 2
- [29] Changhao Shi, Chester Holtz, and Gal Mishne. Online adversarial purification based on self-supervised learning. In *International Conference on Learning Representations*, 2020. 2, 9
- [30] Yang Song, Taesup Kim, Sebastian Nowozin, Stefano Ermon, and Nate Kushman. PixelDefend: Leveraging generative models to understand and defend against adversarial examples. In *International Conference on Learning Representations*, 2018. 2, 9
- [31] David Stutz, Matthias Hein, and Bernt Schiele. Disentangling adversarial robustness and generalization. In *IEEE Conference on Computer Vision and Pattern Recognition*, pages 6976–6987, 2019. 2
- [32] Christian Szegedy, Wojciech Zaremba, Ilya Sutskever, Joan Bruna, Dumitru Erhan, Ian J. Goodfellow, and Rob Fergus. Intriguing properties of neural networks. In *ICLR*, 2014. 1
- [33] Dimitris Tsipras, Shibani Santurkar, Logan Engstrom, Alexander Turner, and Aleksander Madry. Robustness may be at odds with accuracy. In *International Conference on Learning Representations*, 2018. 1
- [34] Matthew J.F. Willetts, Alexander Camuto, Tom Rainforth, S. Roberts, and Christopher C. Holmes. Improving VAEs’ robustness to adversarial attack. In *International Conference on Learning Representations*, 2021. 2
- [35] Eric Wong and Zico Kolter. Provable defenses against adversarial examples via the convex outer adversarial polytope. In *International Conference on Machine Learning*, pages 5286–5295. PMLR, 2018. 1
- [36] Han Xiao, Kashif Rasul, and Roland Vollgraf. Fashion-MNIST: a novel image dataset for benchmarking machine learning algorithms. *arXiv preprint arXiv:1708.07747*, 2017. 4, 5
- [37] Jongmin Yoon, Sung Ju Hwang, and Juho Lee. Adversarial purification with score-based generative models. In *International Conference on Machine Learning*, 2021. 2, 9
- [38] Hongyang Zhang, Yaodong Yu, Jiantao Jiao, Eric Xing, Laurent El Ghaoui, and Michael Jordan. Theoretically principled trade-off between robustness and accuracy. In *International Conference on Machine Learning*, pages 7472–7482. PMLR, 2019. 1, 9
- [39] Jianli Zhou, Chao Liang, and Jun Chen. Manifold projection for adversarial defense on face recognition. In *European Conference on Computer Vision*, 2020. 2

A. Appendix

A.1. Model Architectures and Training Details

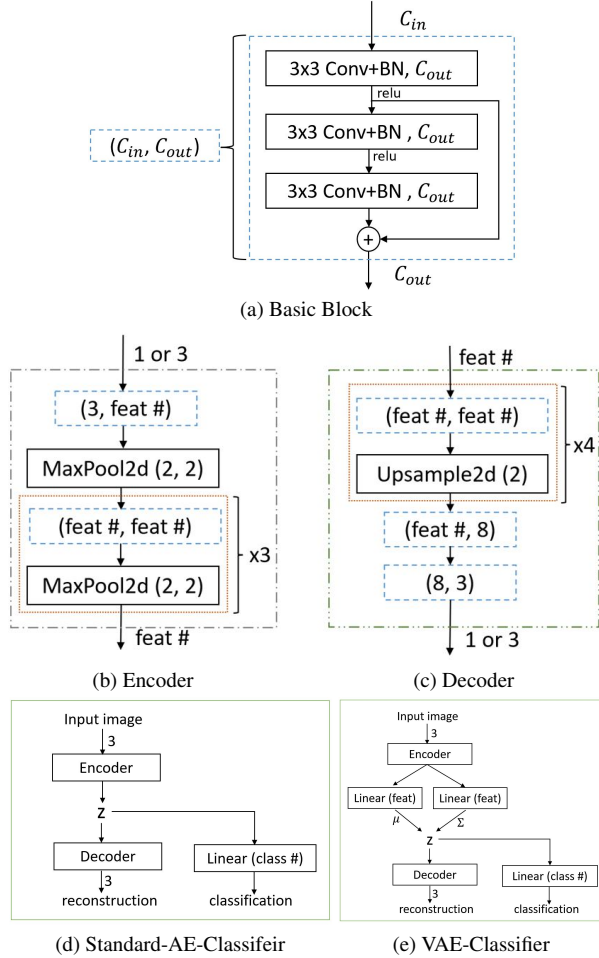


Figure 8. (a) Basic residual block. (b) Encoder. (c) Decoder. (d) Standard-AE-Classifair model. (e) VAE-Classifair model. C_{in} represents number of input feature maps and C_{out} represents number of output feature maps. Number of feature maps is denoted by $feat\#$ in the figure (b) and (c).

We use sequence of residual blocks, as shown in Figure 8(a), to construct the encoder and the decoder. The encoder is consisted of 4 residual blocks as shown in Figure 8(b). The decoder is consisted of 6 residual blocks as shown in Figure 8(c). We set convolution kernel size to 3×3 and use max pooling and upsampling to reduce and increase hidden layer dimensions respectively. Different number of feature maps ($feat\#$) are used to construct models. We use 64 feature maps in each residual block for MNIST and Fashion-MNIST, 128 for SVHN, and 256 for CIFAR-10. A linear classification head is added on top of the latent vector z as shown in Figure 8(d) and (e). During the inference, we use mean values of the encoder’s outputs to replace the

sampling steps of VAE models. We also evaluate our method with larger encoder models such as ResNet-50 (standard training) and PreActResNet-18 (adversarial training). For the adversarially trained model, we freeze the pretrained encoder and train the decoder only.

For MNIST and Fashion-MNIST, we train the model for 256 epochs using the Adam optimizer with a learning rate of 10^{-4} . For SVHN, we train the model for 1024 epochs using the Adam optimizer starting with a learning rate of 10^{-4} and divide it by 10 at the 512th epoch. For CIFAR10, we train the model for 2048 epochs using the Adam optimizer starting with a learning rate of 10^{-4} and divide it by 10 at the 1024th epoch. We set β_1 to 0.9 and β_2 to 0.999 for the optimizer. Batch sizes are set to 256 for all experiments.

A.2. Reconstruction Loss and KL Divergence

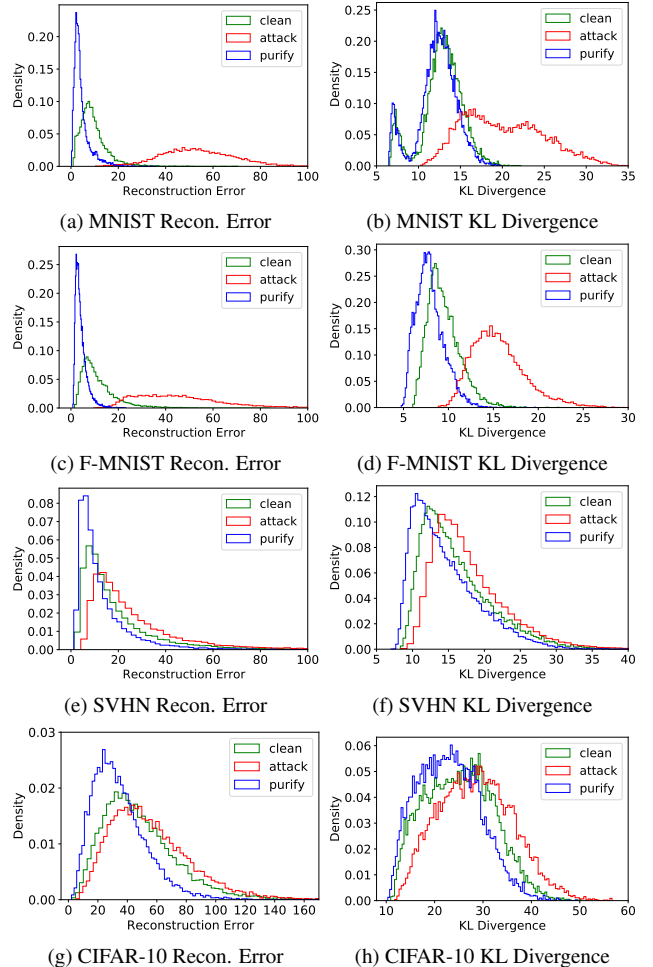
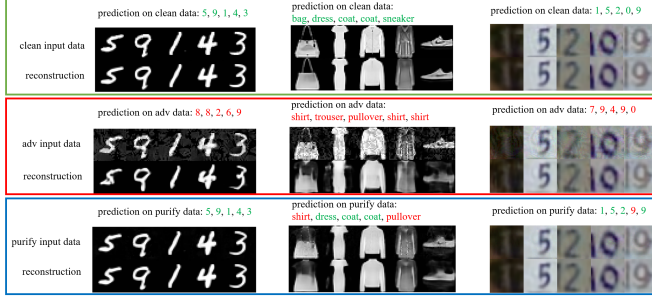


Figure 9. The reconstruction loss and the KL divergence for clean examples, adversarial examples and purified examples.

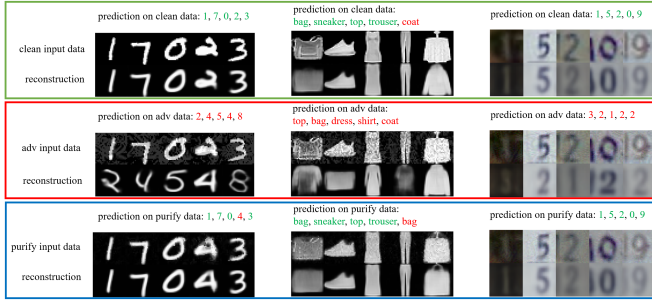
The negative ELBO consists of the reconstruction loss as well as the KL divergence. We observe that adversarial

attacks increase both the reconstruction loss and the KL divergence. We visualize the shifts in Figure 9.

A.3. Reconstruction Outputs between Standard AE Models and Correlated VAE Models



(a) Standard-AE-Classifier



(b) VAE-Classifier

Figure 10. (a) Performance of the Standard-AE-Classifier models on some clean samples (green box), adversarial samples (red box) and purified samples (blue box). (b) Performance of the VAE-Classifier model on some clean samples (green box), adversarial samples (red box) and purified samples (blue box).

Figure 10 shows various sample predictions and reconstructions on clean, attack and purified examples using Standard-AE-Classifier and VAE-Classifier models. For VAE-Classifier models, abnormal reconstructions during attacks are correlated with abnormal predictions from classification heads, which is not hold for standard-AE-Classifier models.